The EMBO Journal Vol. 22 No. 15 pp. 3825–3832, 2003

NFAT functions as a working memory of Ca^{2+} signals in decoding Ca^{2+} oscillation

Taichiro Tomida, Kenzo Hirose, Azusa Takizawa, Futoshi Shibasaki[1] and Masamitsu Iino[2]

Department of Pharmacology, Graduate School of Medicine, The University of Tokyo, Bunkyo-ku, Tokyo 113-0033 and [1]Department of Molecular Cell Physiology, The Tokyo Metropolitan Institute of Medical Science, Bunkyo-ku, Tokyo 113-8613, Japan

[2]Corresponding author
e-mail: iino@m.u-tokyo.ac.jp

Transcription by the nuclear factor of activated T cells (NFAT) is regulated by the frequency of Ca^{2+} oscillation. However, why and how Ca^{2+} oscillation regulates NFAT activity remain elusive. NFAT is dephosphorylated by Ca^{2+}-dependent phosphatase calcineurin and translocates from the cytoplasm to the nucleus to initiate transcription. We analyzed the kinetics of dephosphorylation and translocation of NFAT. We show that Ca^{2+}-dependent dephosphorylation proceeds rapidly, while the rephosphorylation and nuclear transport of NFAT proceed slowly. Therefore, after brief Ca^{2+} stimulation, dephosphorylated NFAT has a lifetime of several minutes in the cytoplasm. Thus, Ca^{2+} oscillation induces a build-up of dephosphorylated NFAT in the cytoplasm, allowing effective nuclear translocation, provided that the oscillation interval is shorter than the lifetime of dephosphorylated NFAT. We also show that Ca^{2+} oscillation is more cost-effective in inducing the translocation of NFAT than continuous Ca^{2+} signaling. Thus, the lifetime of dephosphorylated NFAT functions as a working memory of Ca^{2+} signals and enables the control of NFAT nuclear translocation by the frequency of Ca^{2+} oscillation at a reduced cost of Ca^{2+} signaling.

Keywords: calcineurin/Ca^{2+} oscillation/frequency dependence/NFAT/nuclear translocation

Introduction

An increase in intracellular Ca^{2+} concentration ($[Ca^{2+}]_i$) regulates a vast array of important cellular functions including contraction, secretion, synaptic plasticity, fertilization and immune responses (Clapham, 1995; Berridge *et al*., 2000). The versatility of Ca^{2+} signals is assumed to be dependent on the spatiotemporal patterns of intracellular Ca^{2+} signals. One of the most notable spatiotemporal patterns of Ca^{2+} signals is the oscillatory change in $[Ca^{2+}]_i$, or Ca^{2+} oscillation (Fewtrell, 1993; Berridge *et al*., 2000). Many cellular functions are thought to be regulated by the Ca^{2+} oscillation frequency (Negulescu *et al*., 1994; De Koninck and Schulman, 1998; Dolmetsch *et al*., 1998; Li *et al*., 1998; Oancea and Meyer, 1998). However, the molecular mechanism underlying the Ca^{2+} oscillation frequency dependence of the activation of specific cellular functions has remained elusive.

Gene transcription due to the nuclear factor of activated T cells (NFAT) is one of the cellular responses regulated by Ca^{2+} oscillation frequency (Dolmetsch *et al*., 1998; Li *et al*., 1998). NFAT remains in the cytoplasm when phosphorylated within unstimulated cells. Following an increase in $[Ca^{2+}]_i$, NFAT is dephosphorylated by the Ca^{2+}-dependent phosphatase, calcineurin (Klee *et al*., 1998; Rusnak and Mertz, 2000). Then, NFAT translocates to the nucleus to initiate the transcription of a set of genes (Graef *et al*., 2001). Although several subtypes of NFAT with different tissue distributions have been discovered, conventional NFATs (NFAT1–4) share a common Ca^{2+}-dependent property (Kiani *et al*., 2000). However, the molecular basis of the decoding mechanism of Ca^{2+} oscillation frequency dependence remains to be elucidated. In this study, we carried out continuous imaging of the subcellular distribution of green fluorescent protein (GFP)-tagged NFAT4, while manipulating $[Ca^{2+}]_i$ in a time-controlled manner. We also analyzed the time-course of the Ca^{2+}-dependent NFAT dephosphorylation and compared it with that of nuclear translocation. We show that the lifetime of dephosphorylated NFAT in the cytoplasm is the key factor that determines the Ca^{2+} oscillation frequency dependence of nuclear translocation of NFAT. These results were confirmed by experiments on endogenous NFAT4 in Jurkat T cells. Furthermore, we show that the decoding mechanism makes Ca^{2+} oscillation more advantageous than a continuous increase in $[Ca^{2+}]_i$ in terms of Ca^{2+} signaling efficiency. The present study clarifies the molecular basis and advantage of the decoding mechanism of Ca^{2+} oscillation.

Results and discussion

Time-course of Ca^{2+}-dependent NFAT translocation

We monitored the NFAT translocation into the nucleus following an increase in intracellular Ca^{2+} concentration ($[Ca^{2+}]_i$) in baby hamster kidney (BHK) cells expressing GFP-tagged NFAT4 (GFP–NFAT) (Ho *et al*., 1995; Shibasaki *et al*., 1996). The Ca^{2+}-clamp method (Dolmetsch *et al*., 1998) was used to vary $[Ca^{2+}]_i$, which was simultaneously monitored using a fluorescent Ca^{2+} indicator. Prior to the Ca^{2+} stimulation, a dominant fraction of GFP–NFAT was present in the cytoplasmic region (Figure 1Ai). Following an increase in $[Ca^{2+}]_i$, GFP–NFAT gradually accumulated in the nuclear region with a concomitant decrease in the amount of cytoplasmic GFP–NFAT (Figure 1Aii–iv and B). Notably, the GFP–NFAT translocation lagged significantly behind the increase in $[Ca^{2+}]_i$. This indicates that there is a slow rate-limiting process leading to the nuclear translocation of GFP–NFAT downstream of Ca^{2+} signals. Soon after the

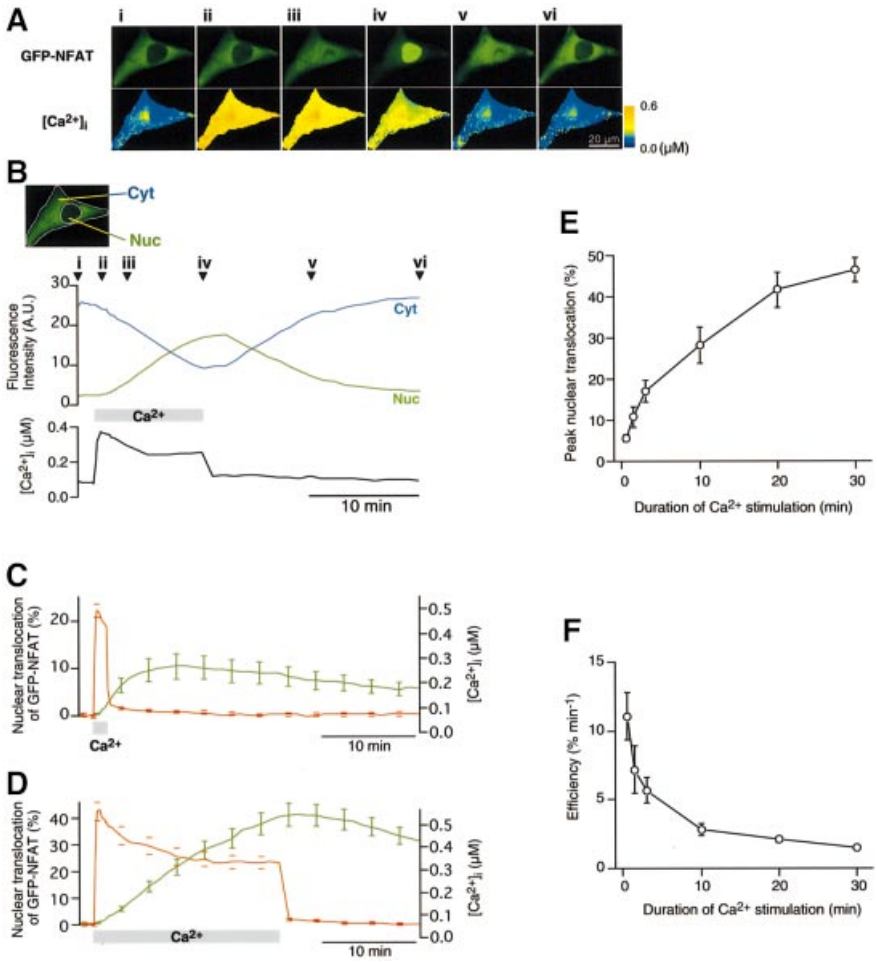

Fig. 1. Imaging of Ca^{2+}-dependent nuclear translocation of GFP–NFAT. (**A**) Time-lapse images of GFP–NFAT and $[Ca^{2+}]_i$ at various time points during and after Ca^{2+} stimulation as indicated in (B). (**B**) Changes in GFP fluorescence intensity of the cell shown in (A) in the cytoplasmic region (indicated as Cyt) and the nuclear region (Nuc) are plotted with the change in $[Ca^{2+}]_i$. (**C** and **D**) Time courses of GFP–NFAT translocation and $[Ca^{2+}]_i$ upon Ca^{2+} stimulation for 1.5 min [(C), n = 10] or 20 min [(D), n = 8] (mean ± SEM). The ranges of errors are shown only at selected time points for clarity. (**E**) Dependence of the peak extent of GFP–NFAT nuclear translocation on the duration of Ca^{2+} stimulation (mean ± SEM; n = 8–21). (**F**) Efficiency of GFP–NFAT nuclear translocation. Peak nuclear translocation of GFP–NFAT per unit duration of Ca^{2+} stimulation was plotted against the duration of Ca^{2+} stimulation.

termination of Ca^{2+} stimulation, the increase in the amount of nuclear GFP–NFAT stopped, and then GFP–NFAT export from the nucleus began (Figure 1Av and vi, and B). On the other hand, GFP expressed in BHK cells exhibited uniform distribution in and out of the nucleus, and no change in the distribution was observed upon Ca^{2+} stimulation (data not shown).

Surprisingly, when brief (1.5 min) Ca^{2+} stimulation was given, the nuclear transport of GFP–NFAT proceeded even after the termination of Ca^{2+} stimulation, reaching a peak ~8 min after Ca^{2+} stimulation (Figure 1C). This result indicates that GFP–NFAT is capable of storing information carried by the transient increase in $[Ca^{2+}]_i$ as a working memory and that the slow GFP–NFAT transport across the nuclear membrane proceeds in a Ca^{2+}-independent manner. We then examined the effects of the duration of Ca^{2+} stimulation on the extent of GFP–NFAT translocation. With 1.5 min of stimulation, ~10% of GFP–NFAT translocated into the nucleus (Figure 1C). When the duration of Ca^{2+} stimulation was increased to 20 min, ~40% of GFP–NFAT translocated into the nucleus (Figure 1D). We varied the duration of Ca^{2+} stimulation between 0.5 and 30 min. The results obtained showed that the peak nuclear translocation of GFP–NFAT increased, but not linearly, with the duration of Ca^{2+} stimulation (Figure 1E). We also examined the nuclear translocation of GFP–NFAT at different $[Ca^{2+}]_i$ and found that the effect of $[Ca^{2+}]_i$ levels off above 0.3 μM (data not shown). Therefore, although there is a gradual decline in $[Ca^{2+}]_i$ during the long Ca^{2+} stimulation (Figure 1D), this should not have any major effects on our results, because $[Ca^{2+}]_i$ was maintained above 0.3 μM.

NFAT dephosphorylation and nuclear translocation

Since NFAT is dephosphorylated by calcineurin before its nuclear translocation, we analyzed the kinetics of dephosphorylation to elucidate the mechanism that dissociates the time courses of $[Ca^{2+}]_i$ and the nuclear translocation of NFAT. At different times after the initiation of Ca^{2+} stimulation, cells were collected to separate cytoplasmic and nuclear fractions. The relative amounts of the phosphorylated and dephosphorylated

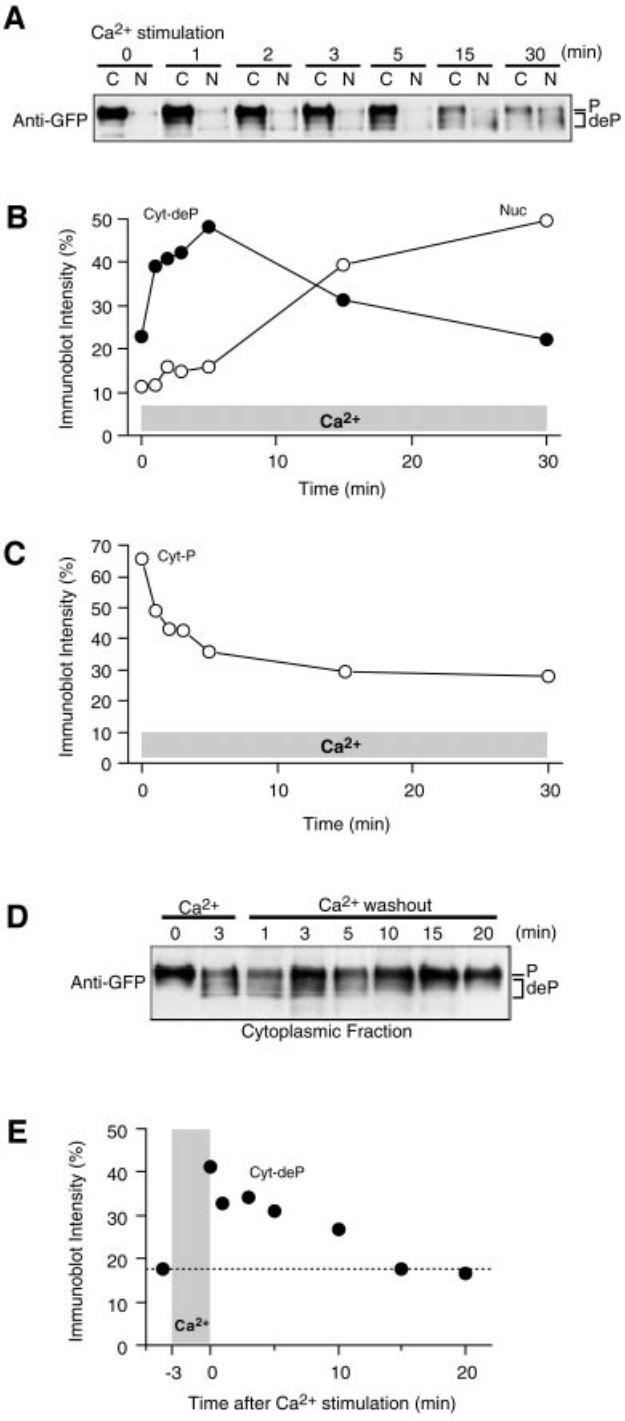

Fig. 2. Analysis of dephosphorylation of GFP–NFAT. (**A**) Dephosphorylation and nuclear translocation of GFP–NFAT upon Ca^{2+} stimulation. The phosphorylation level of GFP–NFAT was analyzed by western blotting with the anti-GFP antibody after the rapid fractionation of BHK cells during Ca^{2+} stimulation. C, cytoplasmic fraction; N, nuclear fraction. Representative results of three experiments. (**B** and **C**) Time-course of the densitometric signals of cytoplasmic-dephosphorylated and nuclear GFP–NFAT (B) and cytoplasmic-phosphorylated GFP–NFAT (C) normalized by total density. (**D**) Decay of dephosphorylated GFP–NFAT in the cytoplasm after the termination of Ca^{2+} signaling. Cells were first stimulated with Ca^{2+} for 3 min, then fractionated at the indicated time-points after Ca^{2+} removal. Representative results of three experiments are shown. (**E**) Time-course of the densitometric signal of cytoplasmic dephosphorylated GFP–NFAT normalized by total density.

forms of GFP–NFAT were determined in each fraction on the basis of the change in the relative molecular weight by SDS–PAGE (Ruff and Leach, 1995; Shibasaki *et al*., 1996). Before Ca^{2+} stimulation, a major GFP–NFAT band with an apparent molecular weight of ~150 kDa was observed in the cytoplasmic fraction (Figure 2A), indicating that the predominant fraction of GFP–NFAT is present in the cytoplasm in a phosphorylated form at rest. Upon Ca^{2+} stimulation, the amount of nuclear GFP–NFAT increased gradually (Figure 2A and B, open circles), with a time-course consistent with that obtained by fluorescence imaging (Figure 1D). In contrast, the amount of dephosphorylated GFP–NFAT rapidly increased in the cytoplasmic fraction within a few minutes after the initiation of Ca^{2+} stimulation, as shown by the increase in the mobility of the GFP–NFAT band, and then gradually decreased (Figure 2A and B, filled circles). The widening of the dephosphorylated band may reflect the presence of multiple phosphorylation sites on each NFAT molecule (Chow *et al*., 1997; Zhu *et al*., 1998; Okamura *et al*., 2000; Marin *et al*., 2002). On the other hand, the amount of phosphorylated GFP–NFAT in the cytoplasm decreased rapidly within 5 min of Ca^{2+} stimulation, but slowly afterwards (Figure 2A and C). These results indicate that GFP–NFAT is rapidly dephosphorylated in the cytoplasm after Ca^{2+} stimulation and becomes nuclear transport ready, but that its nuclear transport proceeds very slowly, causing the temporal dissociation between Ca^{2+} signals and translocation.

We also examined the time-course of the amount of dephosphorylated GFP–NFAT in the cytoplasmic fraction after the termination of brief (3 min) Ca^{2+} stimulation. Dephosphorylated GFP–NFAT remained detectable in the cytoplasm for more than 10 min (Figure 2D and E). This is consistent with the observation that the nuclear translocation of GFP–NFAT continues for several minutes after the termination of brief Ca^{2+} stimulation (Figure 1C). Thus, the dephosphorylated, nuclear-transport-ready GFP–NFAT in the cytoplasm functions as a working memory of Ca^{2+} signals.

Model calculation

For more quantitative analysis, we examined whether we could model the nuclear translocation processes of NFAT. We assumed that NFAT is present in three states (cytoplasmic phosphorylated, cytoplasmic dephosphorylated and nuclear transported) and that there are transitions between the states, as indicated by the arrows in Figure 3A. The transition rate constants were assumed to be constant except for the dephosphorylation rate constant (k_1), which was made to be under on–off regulation by $[Ca^{2+}]_i$. The solutions of two exponential terms can be obtained to describe the time-course of each state by solving differential equations (see Materials and methods). By finding an appropriate set of rate constants, we were able to fit the imaging data with reasonable accuracy using the model (Figure 3B, open circles; see legend for rate constants). Furthermore, the model provided the time-course of the concentration of dephosphorylated, nuclear-transport-ready NFAT (Figure 3B, filled circles), which showed reasonable correlation with the actual measurement of the dephosphorylation time-course during Ca^{2+} stimulation (Figure 2B, filled circles). Therefore, the model is

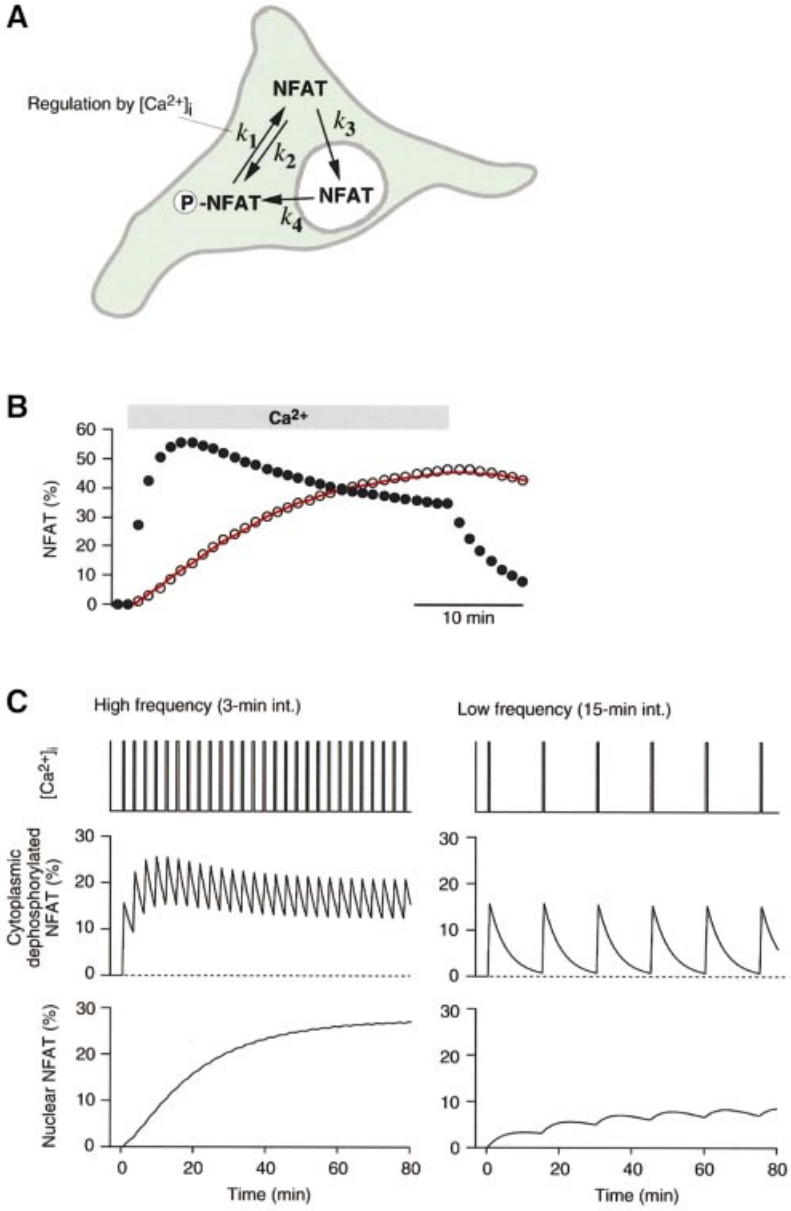

Fig. 3. Model of Ca^{2+}-dependent nuclear translocation of NFAT. (**A**) Schematic illustration of a model of NFAT translocation. NFAT assumes one of the three states, cytoplasmic phosphorylated, cytoplasmic dephosphorylated or nuclear transported. Rate constants are defined as indicated. The dephosphorylation rate constant (k_1) was assumed to be regulated by $[Ca^{2+}]_i$. (**B**) Model fitting (open circles) to the nuclear translocation time-course of NFAT (continuous trace). Model prediction of the time-course of cytoplasmic-dephosphorylated NFAT is also shown (filled circles). Model parameters used: k_1, 0.359/min (during Ca^{2+} stimulation); k_2, 0.147/min; k_3, 0.060/min; and k_4, 0.035/min. (**C**) Model prediction of NFAT translocation during Ca^{2+} oscillation. High-frequency Ca^{2+} oscillation maintains dephosphorylated NFAT in the cytoplasm and induces significant nuclear translocation. Low-frequency oscillation results in intermittent dephosphorylation and induces only slight nuclear translocation of NFAT. Model parameters were the same as those used in (B).

successful in describing the basic features of the Ca^{2+}-dependent nuclear translocation of NFAT.

We further examined the behavior of the model when an oscillatory change in $[Ca^{2+}]_i$ was applied. As shown in Figure 3C (left panel), a high-frequency oscillation of 0.5 min Ca^{2+} spikes maintains NFAT dephosphorylation, since NFAT is repetitively dephosphorylated before the dephosphorylated NFAT (working memory) disappears from the cytoplasm. Therefore, a high-level nuclear translocation occurs. On the other hand, a low-frequency Ca^{2+} oscillation induces the intermittent dephosphorylation of NFAT and a low-level nuclear translocation (Figure 3C, right panel). Thus, the model succeeds in decoding Ca^{2+} oscillation frequency. We then tested these model predictions experimentally.

Ca^{2+} oscillation frequency and nuclear translocation of NFAT

We challenged the cells with Ca^{2+} stimulation of 0.5 min duration at intervals varying between 1.5 and 15 min (Figure 4A), which include the physiological range of Ca^{2+} oscillation intervals observed in activated T cells (Lewis and Cahalan, 1989; Donnadieu *et al.*, 1992). The Ca^{2+} oscillations induced the nuclear translocation of

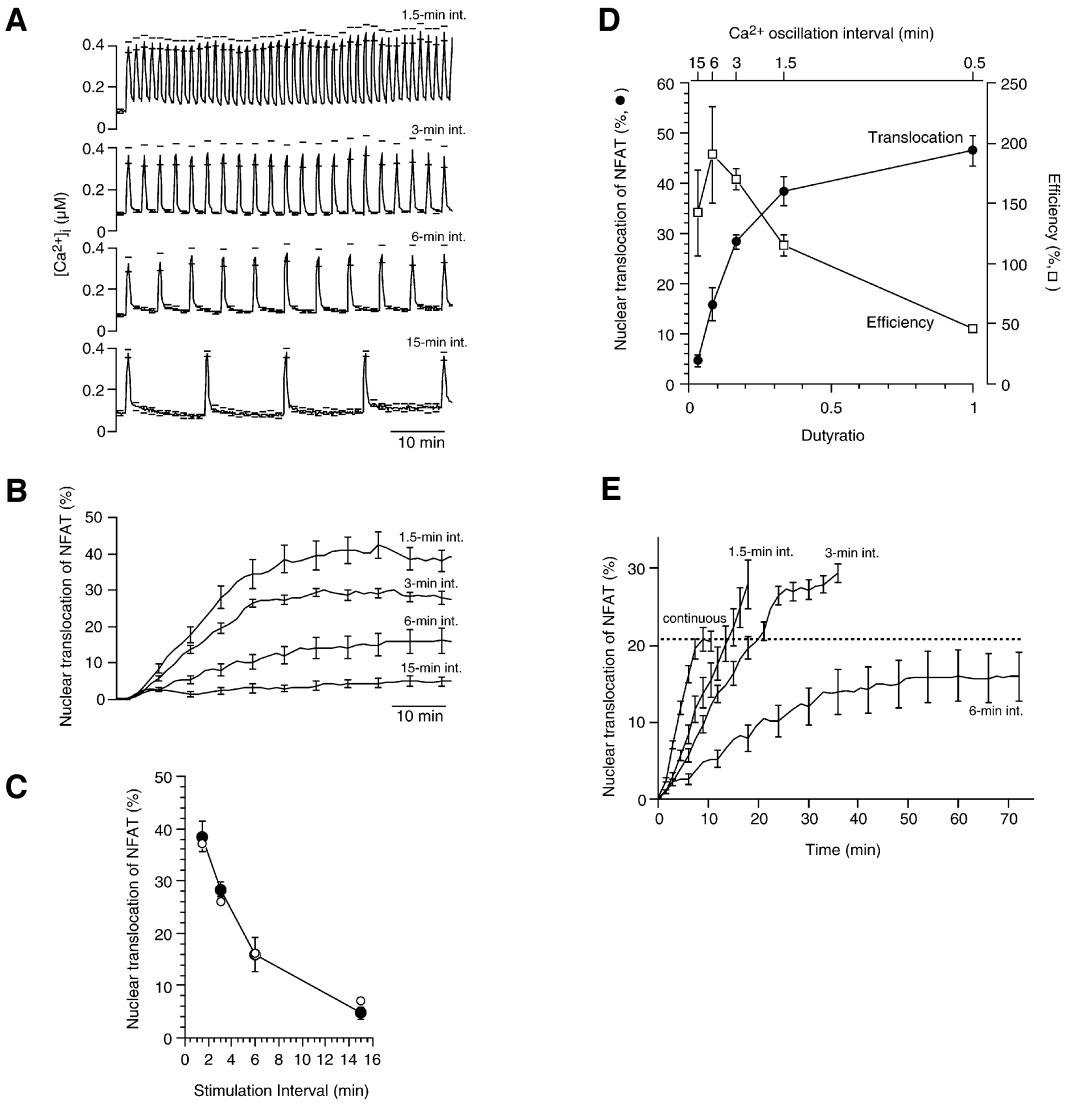

Fig. 4. Ca^{2+} oscillation frequency dependence of GFP–NFAT nuclear translocation. (**A**) $[Ca^{2+}]_i$ in GFP–NFAT expressing BHK cells challenged with Ca^{2+} pulses of 0.5 min duration at different intervals (1.5–15 min). (**B**) GFP–NFAT translocation during oscillatory Ca^{2+} stimulation. Increase in GFP fluorescence intensity of the nuclear region normalized by that of the entire cell region. (**C**) Steady-state nuclear translocation of GFP–NFAT is plotted against Ca^{2+} oscillation interval. Filled circles, experimental results; open circles, model predictions. (**D**) Dependence of nuclear translocation effectiveness and efficiency on the duty ratio of Ca^{2+} oscillation. Filled circles, steady-state nuclear translocation level; open squares, efficiency of Ca^{2+} signals expressed as nuclear translocation divided by duty ratio. (**E**) Nuclear translocation of GFP–NFAT during Ca^{2+} stimulation of the same total duration but different patterns. Ca^{2+} stimulation was applied as either a single continuous 6 min pulse or 12 pulses of 0.5 min duration at intervals of 1.5, 3 or 6 min. The mean ± SEM (n = 5–10) is shown for all results. The ranges of errors are shown only at selected time points for clarity in (A), (B) and (E).

GFP–NFAT in a frequency-dependent manner (Figure 4B). The extent of steady-state nuclear translocation of GFP–NFAT decreased with increasing stimulation interval (Figure 4C, filled circles), in general agreement with the model prediction (Figure 4C, open circles). These results provide direct evidence that NFAT translates different Ca^{2+} oscillation frequencies into its nuclear localization level.

Efficiency of signal transmission and Ca^{2+} oscillation frequency

The generation of Ca^{2+} signals imposes various costs to cells, such as the metabolism of signaling molecules, activation of Ca^{2+} pump ATPase and Ca^{2+}-mediated cell death (Shibasaki and McKeon, 1995; Berridge *et al.*, 1998). It would be beneficial for cells to increase the efficiency of Ca^{2+} signaling to maximize the effect at a minimized cost associated with Ca^{2+} signaling. The efficiency of Ca^{2+} signals was evaluated as the extent of nuclear translocation of GFP–NFAT per unit duration of Ca^{2+} signals, and it decreased with Ca^{2+} signal duration (Figure 1E). Since short Ca^{2+} pulses are more efficient than long Ca^{2+} pulses, it is conceivable that oscillatory changes in $[Ca^{2+}]_i$ can be more efficient than a continuous increase in translocating NFAT. The efficiency of Ca^{2+} oscillation can be evaluated by the extent of steady-state nuclear translocation divided by the duty ratio, which is the ratio of the duration of individual Ca^{2+} stimulation (i.e. 0.5 min in the present experiment) to the oscillation interval and is proportional to the frequency of Ca^{2+} oscillation. Our

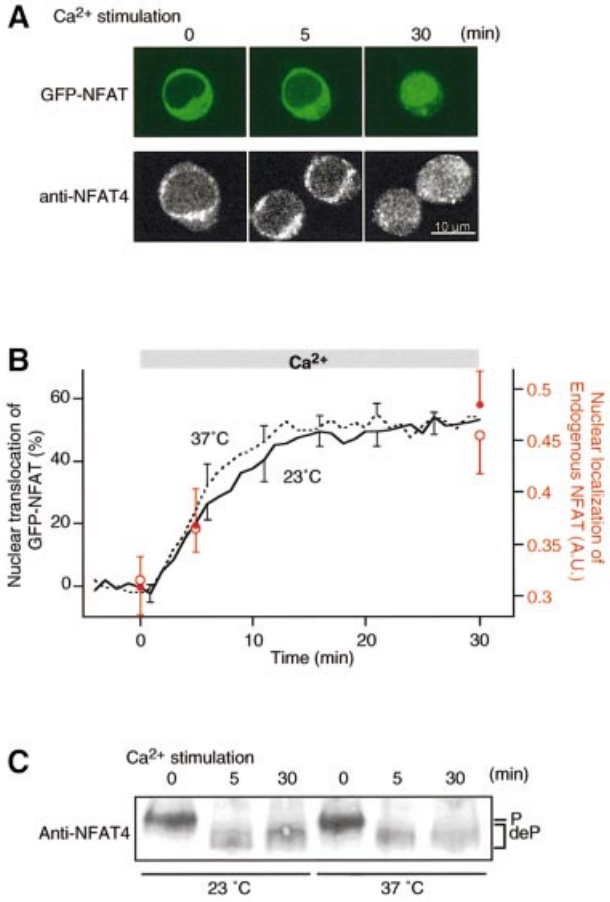

Fig. 5. Activation kinetics of endogenous NFAT in Jurkat T cells. (**A**) Time-lapse images of GFP–NFAT translocation (upper panel) and samples of anti-NFAT4 immunofluorescence images (lower panel) obtained at the indicated time-points after Ca^{2+} stimulation. (**B**) Time courses of nuclear translocation of endogenous NFAT4 (circles) and GFP–NFAT (lines) upon Ca^{2+} stimulation. Experiments were carried out at room temperature (open circles, n = 9–12; continuous line, n = 7) and 37°C (filled circles, n = 11–17; dashed line, n = 6) (mean ± SEM). The ranges of errors are shown only at selected time points for clarity in the GFP–NFAT experiments. (**C**) Dephosphorylation of endogenous NFAT4 following Ca^{2+} stimulation. Whole-cell lysate prepared from Jurkat cells stimulated with Ca^{2+} at either room temperature or 37°C were used for western blotting with rabbit antiserum raised against NFAT4. Dephosphorylation of NFAT4 resulted in the mobility shift of the immunoblot bands.

results show that the extent of nuclear translocation of GFP–NFAT is enhanced with the increase in duty ratio (Figure 4D, filled circles), while the efficiency of Ca^{2+} signaling decreases (Figure 4D, open squares). Thus, Ca^{2+} oscillations with the duty ratios of 0.17 and 0.33 (3 and 1.5 min intervals) resulted in ~60 and 80%, respectively, of the maximum nuclear translocation of GFP–NFAT at more than 3- or 2-fold higher efficiency than continuous Ca^{2+} signaling.

The efficiency of Ca^{2+} oscillation has been analyzed from a different viewpoint. Li *et al*. (1998) studied NFAT-mediated gene expression in response to Ca^{2+} release from intracellular stores due to the photolysis of caged inositol 1,4,5-trisphosphate (IP_3). The same total amount of caged IP_3 elicited a more enhanced gene expression when intermittently photolyzed at 1 min intervals than when photolyzed at shorter or longer intervals, or continuously. This study suggests that the effect of Ca^{2+} oscillation can be maximized within a certain range of frequencies at the same cost of IP_3 generation. However, the mechanism underlying this phenomenon has not been elucidated. We carried out experiments along this line, and Ca^{2+} stimulation of the same total duration was applied to the cells as either a single continuous 6 min stimulation or 12 pulses of 0.5 min duration at intervals of 1.5, 3 or 6 min. Ca^{2+} oscillation at 1.5 or 3 min intervals produced a higher-peak nuclear translocation of GFP–NFAT than the continuous increase or oscillation at 6 min intervals (Figure 4E). These results demonstrate that the cost-effectiveness of Ca^{2+} signaling increases during Ca^{2+} oscillation at optimal frequencies. For this property of the Ca^{2+}-oscillation-mediated regulation of cell functions, the presence of a working memory is essential. If there were no working memory, i.e. if the nuclear translocation of NFAT proceeded only during $[Ca^{2+}]_i$ increase, the maximum nuclear translocation would be limited by the total duration of $[Ca^{2+}]_i$ increase. Under such conditions, oscillatory increases in $[Ca^{2+}]_i$ would always cause a lower extent of final nuclear transport than a continuous increase in $[Ca^{2+}]_i$, because NFAT would escape from the nucleus during interoscillation periods.

Ca^{2+}-dependent translocation of endogenous NFAT in Jurkat T cells

We examined whether the properties of exogenously expressed GFP-tagged NFAT are applicable to the physiological behavior of endogenous NFAT. Since endogenous NFAT4 is expressed in the human T cell line, Jurkat (Lyakh *et al*., 1997), we compared Ca^{2+}-dependent nuclear translocation of endogenous NFAT with that of GFP–NFAT expressed in these cells. GFP–NFAT expressed in Jurkat cells also showed cytoplasmic localization at rest (Figure 5A, upper panel). Upon Ca^{2+} stimulation, GFP–NFAT gradually translocated into the nucleus (Figure 5A and B, continuous line), and the time-course was similar to that of GFP–NFAT expressed in BHK cells (Figure 1D). We then observed the translocation of endogenous NFAT by performing anti-NFAT4 immunostaining at various time points after Ca^{2+} stimulation. Endogenous NFAT also showed cytoplasmic localization at rest (Figure 5A, lower panel). Upon Ca^{2+} stimulation, nuclear staining intensity increased with a time-course similar to that of GFP–NFAT expressed in Jurkat cells (Figure 5A, lower panel, and B, red open symbols). We also carried out the same experiments at 37°C and found approximately the same time-course between the nuclear translocation of GFP–NFAT (Figure 5B, dashed line) and that of endogenous NFAT (Figure 5B, red filled symbols). We further examined the kinetics of dephosphorylation of endogenous NFAT upon Ca^{2+} stimulation. Endogenous NFAT4 was rapidly dephosphorylated within 5 min of Ca^{2+} stimulation at both room temperature and 37°C (Figure 5B), as was the case with GFP–NFAT in BHK cells at room temperature (Figure 2). These results demonstrate that endogenous NFAT in Jurkat cells undergoes rapid dephosphorylation and slow nuclear translocation, as seen in GFP–NFAT expressed in either BHK cells or Jurkat cells. We observed in Jurkat cells parallel increases in the steady-state endogenous NFAT translocation and NFAT reporter gene activity with

increasing amplitude of Ca^{2+} stimulation (data not shown). Indeed, the oscillation interval dependence of nuclear translocation (Figure 4C) is generally consistent with that of the expression of an NFAT reporter gene in Jurkat cells (Dolmetsch *et al*., 1998).

Ca^{2+} oscillation frequency-dependent translocation of NFAT

The present results clarified the molecular basis of the decoding mechanism of Ca^{2+} oscillation by NFAT. NFAT is rapidly dephosphorylated upon an increase in $[Ca^{2+}]_i$ and a significant fraction of NFAT becomes nuclear transport ready. Since the rephosphorylation of NFAT in the cytoplasm proceeds slowly even after a brief Ca^{2+} stimulation, dephosphorylated transport-ready NFAT remains in the cytoplasm for several minutes and functions as a working memory of Ca^{2+} signals. However, transport across the nuclear membrane proceeds extremely slow and each transport-ready NFAT molecule has a low chance of undergoing nuclear translocation. When Ca^{2+} stimuli are repeatedly applied at an interval shorter than the lifetime of dephosphorylated NFAT, there is a build-up of transport-ready NFAT in the cytoplasm. This promotes the nuclear translocation of NFAT during Ca^{2+} oscillation. Furthermore, our results demonstrated that, due to the presence of a working memory, Ca^{2+} oscillation can be more cost-effective for the cell than a continuous increase in $[Ca^{2+}]_i$.

In conclusion, the present study shows that the working memory of brief Ca^{2+} signaling (as a modification of NFAT phosphorylation) upstream of a rate-limiting step plays a key role in decoding Ca^{2+} oscillation frequency and improving the efficiency of Ca^{2+} signaling. This principle may be applicable to other cellular functions that are regulated by Ca^{2+} oscillation.

Materials and methods

Cells and transfection

BHK cells were maintained in modified Eagle's medium (Gibco-BRL, Gaithersberg, MD) containing 5% fetal calf serum (FCS) and supplemented with 100 U/ml penicillin and 100 μg/ml streptomycin. The transfection of pCMV-GFP-NFAT4 (Shibasaki *et al*., 1996) or pCMV-GFP was carried out by the calcium-phosphate method (Shibasaki and McKeon, 1995). Jurkat cells (E6-1) were maintained in RPMI medium (Gibco-BRL) containing 10% FCS and supplemented with 100 U/ml penicillin and 100 μg/ml streptomycin. The transfection of pCMV-GFP-NFAT4 was carried out using LipofectAMINE 2000 (Invitrogen, Carlsbad, CA). Cells were cultured for 30 h after transfection before use.

Fluorescence imaging

GFP–NFAT expressing BHK cells on poly-D-lysine-coated glass-bottomed dish (MatTek, Ashland, MA) were loaded at room temperature with 5 μM Fura-PE3AM (TefLabs, Austin, TX) in physiological salt solution (PSS) containing 150 mM NaCl, 4 mM KCl, 2 mM $CaCl_2$, 1 mM $MgCl_2$, 5.6 mM glucose, 5 mM HEPES pH 7.4 and 5% FCS. The fluorescence images were captured with an inverted microscope (IX70; Olympus, Tokyo, Japan), equipped with a 100× objective (NA 1.35), a cooled charge-coupled device (CCD) camera (Photometrics, Tucson, AZ) and a polychromatic illumination system (T.I.L.L. Photonics, Planegg, Germany), at a rate of one triplet of frames for every 10 s at excitation wavelengths of 355 and 380 nm for Fura-PE3 and 470 nm for GFP. The image-capture interval was changed to 60 s after the Fura-PE3 signal reached the steady-state level. Nuclear translocation of GFP–NFAT was evaluated based on the ratio of the fluorescence intensity of the nuclear region to the fluorescence intensity of the entire region of the cell. The intracellular Ca^{2+} concentration of the Fura-PE3-loaded cells was calculated using a previously reported equation (Grynkiewicz *et al*., 1985). All experiments using BHK cells were carried out at room temperature (23°C).

Jurkat cells expressing GFP–NFAT were adhered onto poly-D-lysine-coated glass-bottomed dish by low-speed centrifugation (200 *g* for 4 min). The fluorescence images were captured every 60 s using a confocal microscope (Fluoview; Olympus) equipped with a 100× objective (NA 1.35) with excitation at 488 nm. Experiments were carried out at either room temperature or 37°C. The nuclear translocation of GFP–NFAT was evaluated based on the ratio of the fluorescence intensity of the nuclear region to that of the entire region of the cell on a confocal plane.

Ca^{2+}-clamp method

$[Ca^{2+}]_i$ was controlled by the Ca^{2+}-clamp method (Dolmetsch *et al*., 1998). Briefly, cells were pretreated with 1 μM thapsigargin to deplete the intracellular Ca^{2+} store and to activate store-operated Ca^{2+} channels. For the regulation of $[Ca^{2+}]_i$ during fluorescence imaging, a computer-controlled puffing pipette was used to treat the cells with PSS containing either 10 mM Ca^{2+} to increase $[Ca^{2+}]_i$ or 5 mM EGTA to decrease $[Ca^{2+}]_i$. When clamping of $[Ca^{2+}]_i$ at intermediate concentrations was necessary, PSS containing <10 mM Ca^{2+} was used. For experiments at 37°C, the bath solution was warmed using a stage heater (Kitazato Supply, Tokyo, Japan) and the puffing solution was also prewarmed.

Cell fractionation

BHK cells were grown on 12-well culture plates, and the bath solution was rapidly changed to control $[Ca^{2+}]_i$ using the Ca^{2+}-clamp method. At various time-points during Ca^{2+} stimulation, the cells were washed with ice-cold phosphate-buffered saline (PBS) and resuspended in prechilled lysis buffer (10 mM NaCl, 0.5 mM dithiothreitol, and 20 mM Tris–Cl, pH 7.5) supplemented with protease inhibitors (complete protease inhibitor cocktail; Roche, Mannheim, Germany), 1 μM pepstatin and 0.1% Nonidet P-40. The cells were then transferred to microcentrifuge tubes, vortexed for 10 s, and centrifuged for 15 s at 17 400 *g*. The supernatant was recovered as a cytoplasmic fraction. The pellet was washed in the above buffer minus the detergent, and resuspended as the nuclear fraction in a buffer containing 0.1% Nonidet P-40. Both fractions were immediately mixed with one-third volume of 4× SDS sample buffer (8% SDS, 20% sucrose, 20% mercaptoethanol, 0.008% bromophenol blue and 250 mM Tris–HCl pH 6.8) and the mixture was boiled at 95°C for 10 min. Equivalent amounts of cytoplasmic and nuclear fractions from ~3×10^5 cells were electrophoresed on 8.5% SDS–polyacrylamide gels and subjected to western blotting. The purity of the fractions were checked by western blotting using the antibodies against HSP90 (cytoplasmic marker) and Sp-1 (nuclear marker) (Santa Cruz Biotechnology, Santa Cruz, CA), and 86.4 ± 1.4% (mean ± SEM, n = 15) Sp-1 was recovered in the nuclear fraction, and 88.6 ± 1.6% (n = 15) HSP90 in the cytoplasmic fraction.

Western blotting

After electrophoresis, the proteins were transferred onto a PVDF membrane (Bio-Rad, Hercules, CA), and non-specific sites were blocked with 5% non-fat dry milk in Tris-buffered saline (100 mM NaCl and 20 mM Tris–HCl pH 7.8). For the detection of GFP–NFAT, the blot was probed with 1:3000 anti-GFP polyclonal antibody (MBL, Nagoya, Japan) and 1:8000 anti-rabbit IgG horseradish peroxidase (MBL) diluted in the blocking buffer, then developed using chemiluminescence reagents (Western Lightning™; PerkinElmer Life Sciences, Boston, MA). The quantitative determination of the immunoblot signal intenisty was carried out using Mac BAS software (Fuji Film, Tokyo, Japan). NFAT dephosphorylation and nuclear translocation were analyzed based on the relative immunoblot intensity of cytoplasmic phosphorylated form, dephosphorylated form and nuclear form. For the analysis of endogenous NFAT in Jurkat cell lysate, proteins were probed with 1:2000 rabbit antiserum raised against recombinant human NFAT4 protein and 1:8000 anti-rabbit IgG conjugated with horseradish peroxidase (MBL).

Model calculation

A model of NFAT translocation is described in the text (see Figure 3A). Designating the fractions of cytoplasmic-phosphorylated NFAT, cytoplasmic-dephosphorylated NFAT and nuclear-transported NFAT as x, y and $1 - x - y$, respectively, we obtained the following differential equations:

$$dx/dt = -k_1 x + k_2 y + k_4 (1 - x - y)$$

$$dy/dt = k_1 x - (k_2 + k_3) y$$

where k_1 is assumed to be 0 in the absence of Ca^{2+} stimulation. Analytical solutions for x and y were obtained using the initial conditions that $x = 1$ and $y = 0$ at $t = 0$, and were fitted to the time-course of the nuclear translocation of GFP–NFAT (Figure 1D) to estimate k_1, k_2, k_3 and k_4. KaleidaGraph (Synergy Software, Reading, PA) and Mathematica (Wolfram Research, Champaign, IL) were used for curve fitting and numerical calculations.

Immunocytochemistry and reporter gene assay

Jurkat cells adhering to the poly-D-lysine-coated glass-bottomed dish were stimulated by the Ca^{2+}-clamp method. After stimulation, the cells were rapidly washed with ice-cold PBS, then fixed with 4% paraformaldehyde, and permeabilized with 0.1% Triton X-100. After blocking with 5% bovine serum albumin in PBS, endogenous NFAT was detected using anti-NFAT4 rabbit antiserum and Alexa 546-conjugated anti-rabbit IgG antibody (Molecular Probes, Eugene, OR). NFAT subcellular localization was visualized with a confocal laser-scanning microscope (Fluoview; Olympus). For evaluating NFAT localization, the fluorescence intensity of the nuclear region was normalized by that of the entire cell region. NFAT transcription activity was studied in Jurkat cells transfected with an NFAT luciferase reporter plasmid. After Ca^{2+} stimulation in the presence of PMA (50 ng/ml) for 3 h at 37°C, the cells were subjected to luciferase assay.

Analysis of endogenous NFAT dephosphorylation

Jurkat cells were stimulated by the Ca^{2+}-clamp method in the presence of 5% FCS. The reaction was stopped by placing on ice and the cells were rapidly pelletted (17 500 *g* for 15 s). The cell pellet was washed once with ice-cold PBS and lysed in preheated (70°C) SDS sample buffer and boiled at 95°C for 10 min. The samples of the whole-cell lysate from ~7.5×10^5 cells were electrophoresed on 8.5% SDS–polyacrylamide gels and subjected to western blotting.

Acknowledgements

We thank Drs A.Hashimoto and S.Namiki for reading the manuscript. This work was supported by grants from the Ministry of Education, Culture, Sports, Science and Technology.

References

Berridge,M.J., Bootman,M.D. and Lipp,P. (1998) Calcium—a life and death signal. *Nature*, **395**, 645–648.

Berridge,M.J., Lipp,P. and Bootman,M.D. (2000) The versatility and universality of calcium signalling. *Nat. Rev. Mol. Cell. Biol.*, **1**, 11–21.

Chow,C.W., Rincon,M., Cavanagh,J., Dickens,M. and Davis,R.J. (1997) Nuclear accumulation of NFAT4 opposed by the JNK signal transduction pathway. *Science*, **278**, 1638–1641.

Clapham,D.E. (1995) Calcium signaling. *Cell*, **80**, 259–268.

De Koninck,P. and Schulman,H. (1998) Sensitivity of CaM kinase II to the frequency of Ca^{2+} oscillations. *Science*, **279**, 227–230.

Dolmetsch,R.E., Xu,K. and Lewis,R.S. (1998) Calcium oscillations increase the efficiency and specificity of gene expression. *Nature*, **392**, 933–936.

Donnadieu,E., Cefai,D., Tan,Y.P., Paresys,G., Bismuth,G. and Trautmann,A. (1992) Imaging early steps of human T cell activation by antigen-presenting cells. *J. Immunol.*, **148**, 2643–2653.

Fewtrell,C. (1993) Ca^{2+} oscillations in non-excitable cells. *Annu. Rev. Physiol.*, **55**, 427–454.

Graef,I.A., Chen,F. and Crabtree,G.R. (2001) NFAT signaling in vertebrate development. *Curr. Opin. Genet. Dev.*, **11**, 505–512.

Grynkiewicz,G., Poenie,M. and Tsien,R.Y. (1985) A new generation of Ca^{2+} indicators with greatly improved fluorescence properties. *J. Biol. Chem.*, **260**, 3440–3450.

Ho,S.N., Thomas,D.J., Timmerman,L.A., Li,X., Francke,U. and Crabtree,G.R. (1995) NFATc3, a lymphoid-specific NFATc family member that is calcium-regulated and exhibits distinct DNA binding specificity. *J. Biol. Chem.*, **270**, 19898–19907.

Kiani,A., Rao,A. and Aramburu,J. (2000) Manipulating immune responses with immunosuppressive agents that target NFAT. *Immunity*, **12**, 359–372.

Klee,C.B., Ren,H. and Wang,X. (1998) Regulation of the calmodulin-stimulated protein phosphatase, calcineurin. *J. Biol. Chem.*, **273**, 13367–13370.

Lewis,R.S. and Cahalan,M.D. (1989) Mitogen-induced oscillations of cytosolic Ca^{2+} and transmembrane Ca^{2+} current in human leukemic T cells. *Cell Regul.*, **1**, 99–112.

Li,W., Llopis,J., Whitney,M., Zlokarnik,G. and Tsien,R.Y. (1998) Cell-permeant caged InsP3 ester shows that Ca^{2+} spike frequency can optimize gene expression. *Nature*, **392**, 936–941.

Lyakh,L., Ghosh,P. and Rice,N.R. (1997) Expression of NFAT-family proteins in normal human T cells. *Mol. Cell. Biol.*, **17**, 2475–2484.

Marin,O., Burzio,V., Boschetti,M., Meggio,F., Allende,C.C., Allende,J.E. and Pinna,L.A. (2002) Structural features underlying the multisite phosphorylation of the A domain of the NF-AT4 transcription factor by protein kinase CK1. *Biochemistry*, **41**, 618–627.

Negulescu,P.A., Shastri,N. and Cahalan,M.D. (1994) Intracellular calcium dependence of gene expression in single T lymphocytes. *Proc. Natl Acad. Sci. USA*, **91**, 2873–2877.

Oancea,E. and Meyer,T. (1998) Protein kinase C as a molecular machine for decoding calcium and diacylglycerol signals. *Cell*, **95**, 307–318.

Okamura,H. *et al.* (2000) Concerted dephosphorylation of the transcription factor NFAT1 induces a conformational switch that regulates transcriptional activity. *Mol. Cell*, **6**, 539–550.

Ruff,V.A. and Leach,K.L. (1995) Direct demonstration of NFATp dephosphorylation and nuclear localization in activated HT-2 cells using a specific NFATp polyclonal antibody. *J. Biol. Chem.*, **270**, 22602–22607.

Rusnak,F. and Mertz,P. (2000) Calcineurin: form and function. *Physiol. Rev.*, **80**, 1483–1521.

Shibasaki,F. and McKeon,F. (1995) Calcineurin functions in Ca^{2+}-activated cell death in mammalian cells. *J. Cell Biol.*, **131**, 735–743.

Shibasaki,F., Price,E.R., Milan,D. and McKeon,F. (1996) Role of kinases and the phosphatase calcineurin in the nuclear shuttling of transcription factor NF-AT4. *Nature*, **382**, 370–373.

Zhu,J., Shibasaki,F., Price,R., Guillemot,J.C., Yano,T., Dotsch,V., Wagner,G., Ferrara,P. and McKeon,F. (1998) Intramolecular masking of nuclear import signal on NF-AT4 by casein kinase I and MEKK1. *Cell*, **93**, 851–861.

Received March 12, 2003; revised June 2, 2003; accepted June 11, 2003